Optical properties of Bi_{2}Te_{2}Se at ambient and high pressures

Ana Akrap, Michaël Tran, Alberto Ubaldini, Jérémie Teyssier, Enrico Giannini, Dirk van der Marel, Philippe Lerch, and Christopher C. Homes

Optical properties of Bi_2Te_2Se at ambient and high pressure

Ana Akrap,[*] Michaël Tran, Alberto Ubaldini, Jérémie Teyssier, Enrico Giannini, and Dirk van der Marel

University of Geneva, CH-1211 Geneva 4, Switzerland

Philippe Lerch

Paul Scherrer Institute, 5232 Villigen, Switzerland

Christopher C. Homes[†]

Condensed Matter Physics and Materials Sciences Department,
Brookhaven National Laboratory, Upton New York, 11973, USA

(Dated: December 3, 2012)

The temperature dependence of the complex optical properties of the three-dimensional topological insulator Bi_2Te_2Se is reported for light polarized in the *a-b* planes at ambient pressure, as well as the effects of pressure at room temperature. This material displays a semiconducting character with a bulk optical gap of $E_g \simeq 300$ meV at 295 K. In addition to the two expected infrared-active vibrations observed in the planes, there is additional fine structure that is attributed to either the removal of degeneracy or the activation of Raman modes due to disorder. A strong impurity band located at $\simeq 200$ cm^{-1} is also observed. At and just above the optical gap, several interband absorptions are found to show a strong temperature and pressure dependence. As the temperature is lowered these features increase in strength and harden. The application of pressure leads to a very abrupt closing of the gap above 8 GPa, and strongly modifies the interband absorptions in the mid-infrared spectral range. While *ab initio* calculations fail to predict the collapse of the gap, they do successfully describe the size of the band gap at ambient pressure, and the magnitude and shape of the optical conductivity.

PACS numbers: 72.20,-i, 74.62.Fj, 78.20.-e

I. INTRODUCTION

A topological insulator is a material in which a large spin-orbit interaction produces a band inversion over a bulk band gap, resulting in protected metallic surface states.[1–3] In the search for three dimensional topological insulators, the discovery of the layered bismuth chalcogenide $Bi_2Te_{3-x}Se_x$ family was of particular importance.[4,5] The simple structure of the surface states in these compounds, with only one Dirac cone traversing the band gap,[6,7] has attracted a great deal of interest. The suitably-sized bulk band gap $(150 - 300$ meV) and robust metallic surface states persisting up to high temperatures[7] make this series of compounds interesting for experimental investigation, and potentially also in applications. However, difficulties concerning material purity and stoichiometry lead to a deteriorated insulating character of the bulk. Bismuth and tellurium have very similar electronegativity on Pauling's scale,[8] and this naturally leads to a large concentration of antisite defects. Bi_2Te_3 is not a line compound but exists in a narrow field of compositions $(\sim 1\%)$;[9] as a result, a slight deficiency or excess of Te will result in either a *p*-type or *n*-type material, respectively.[10] Very often it is the case that Bi_2Te_3 crystals are *p*-type and have a high hole concentration because of a large number of negatively charged defects due to tellurium sites occupied by bismuth atoms.[11] In Bi_2Se_3, on the other hand, because of the high fugacity of selenium, the concentration of selenium vacancies exceeds the concentration of

antisite defects, so that the $Bi_{2+x}Se_3$ crystal typically exhibits *n*-type conductivity.[12,13] All of these factors cause disorder (impurities) in the structure and lead to symmetry breaking and intrinsic doping. Contrary to the expected insulating state, a finite residual conductivity appears. The salient question is how to optimize these systems and decrease the bulk conductivity.

In an ordered stoichiometric structure Se vacancies can be decreased, and the Se/Te randomness diminished. Recently, it was found that Bi_2Te_2Se has the highest resistivity within the $Bi_2Te_{3-x}Se_x$ family. Shubnikov–de Haas oscillations were observed and attributed to the surface states,[14–17] and a single Dirac cone crosses the Fermi surface.[18] Angle-resolved photoemission spectroscopy (ARPES) shows narrow linewidths of topological surface states, which indicates that the disorder is suppressed.[19,20]

To improve existing topological insulators and design new ones, it is necessary to understand the details of their band structure. It is important to know how the impurities influence the conductivity, and what happens if the lattice dimensions are varied, for example, through chemical substitutions. Much of this can be addressed through a careful study of the optical properties. The optical properties of Bi_2Te_3 and Bi_2Se_3 crystals have been intensely studied in the past century.[21] More recently, this family of compounds has been revisited in light of the topological properties.[22,23] In this paper we focus on Bi_2Te_2Se and investigate the temperature dependence of the complex optical properties in order to improve

the understanding of the bulk response. Through room-temperature reflection and transmission experiments at ambient and high pressure, information is obtained about the nature of the band gap, residual conductivity, vibrational modes, and interband transitions. The application of pressure allows the band gap to be studied as the distance between the layers is decreased.

We observe a semiconducting response in the optical conductivity of Bi_2Te_2Se with a gap of $E_g \simeq 2400$ cm^{-1} (0.3 eV); below the gap are two strong infrared-active phonons at $\simeq 62$ and 118 cm^{-1}, an impurity band centered at $\simeq 200$ cm^{-1}, as well as other weaker features. In addition, there is evidence of a low-energy impurity band at $30 - 40$ cm^{-1}, in agreement with a small transport gap extracted from the dc conductivity measurement. The low-energy interband absorptions display a pronounced temperature dependence. The application of pressure with a diamond-anvil cell in Bi_2Te_2Se reduces the inter-layer spacing, altering the band structure. The optical gap is at first unchanged, and then strongly reduced upon pressure increase. Reflectance studies reveal that the band structure is altered by the application of even a small amount of pressure. *Ab initio* calculations of the electronic structure and the optical conductivity confirm the sensitivity of interband absorptions to c-axis compression. However, the calculations show that c-axis compression has very little effect on the band gap.

II. EXPERIMENT AND CALCULATION

Single crystals of Bi_2Te_2Se were grown by the floating zone method starting from the stoichiometric ratio of metallic bismuth and chalcogenide elements. Cleaving the crystal exposes lustrous mirror-like surfaces, which flake off very easily.

The structure of Bi_2Te_2Se is described by the trigonal space group $R\bar{3}m$ (kawazulite) and shown in the inset of Fig. 1. The unit cell consists of quintuple Te–Bi–Se–Bi–Te layers stacked along the c-axis direction.[24,25] The quintuple layers are bound by weak van der Waals interaction, which is responsible for the extreme ease with which the sample may be cleaved.

The temperature-dependent reflectance at ambient pressure was measured at a near-normal angle of incidence on a freshly-cleaved surface for light polarized in the a-b planes, from $\simeq 12$ to over $42\,000$ cm^{-1} (1.5 meV – 5.2 eV) using an *in situ* evaporation technique.[26] The reflectance is a complex quantity, $\tilde{r} = \sqrt{R}e^{i\theta}$; however, only the amplitude R is measured in this experiment. To obtain the phase we employ the Kramers-Kronig relation[27] using suitable extrapolations for the reflectance in the $\omega \rightarrow 0, \infty$ limits. At low frequencies the metallic Hagen-Rubens form for the reflectance $R(\omega) \propto 1 - \sqrt{\omega}$ is employed. Above the highest measured frequency point the reflectance is assumed to be constant up to $\simeq 8 \times 10^4$ cm^{-1}, above which a free electron gas asymptotic reflectance extrapolation $R(\omega) \propto 1/\omega^4$ is

assumed.[28]

Raman spectra were collected using a home-made micro Raman spectrometer equipped with an argon laser at a wavelength of 514.5 nm, a half-meter monochromator and a liquid nitrogen-cooled CCD detector. The spectral resolution was of the order of 1 cm^{-1}. The sample was mounted in a helium-flow cryostat allowing measurements down to 6 K with a long working distance 63$\times$ objective.

Optical data at high pressure were recorded using a diamond anvil cell operated in transmission and reflection geometry. Type IIa diamonds with a culet of 0.55 mm were used with CuBe gaskets with a hole diameter of 250 μm to apply pressures of up to 15 GPa inside a membrane-driven diamond anvil cell. Samples of Bi_2Te_2Se were cleaved to a thickness of a few microns. A fine dry KBr powder was used as the pressure-transmitting medium, and the pressure was monitored *in situ* through ruby fluorescence.[29] In the transmission geometry, light is focused on the sample in a home-made transmission setup with a pair of reflective objectives with a magnification coefficient of 15 and numerical aperture 0.5. For the reflectivity measurement, a Bruker Hyperion 3000 microscope was used with a single 15$\times$ reflective objective. Infrared radiation was provided by the Swiss synchrotron light source (SLS) and coupled[30] to the Fourier transform spectrometer. The high-brightness provided by the synchrotron source allows a spatial resolution of $30 \times 30 \,\mu$m^2 or better while maintaining high throughput.

The band structure was calculated for the primitive cell containing 5 atoms. We used a full-potential linear muffin-tin-orbital (LMTO) program[31] within a local spin-density approximation (LSDA) and generalized gradient approximation (GGA).[32] The effect of spin-orbit coupling was taken into account.[33,34] The k-mesh was $40 \times 40 \times 40$ for the self consistency calculation, and $12 \times 12 \times 12$ for the calculation of the optical conductivity. The energy cutoff was set at 730 eV, and the convergence criterium is such that total energy accuracy is better than 10^{-6} eV.

III. RESULTS AND DISCUSSION

The resistivity measured in the a-b plane is shown in Fig. 1 in an Arrhenius plot (log ρ_{ab} against $1/T$). At 5 K, $\rho_{ab} \simeq 0.16\,\Omega$ cm. From room temperature down to ~ 170 K the behavior of the resistivity is similar to that of a bad metal. The value of ρ_{ab} at room temperature is $\simeq 16$ mΩ cm, and the temperature slope is small and positive, $\simeq 1.3 \times 10^{-5}\,\Omega$ cm/K. Between 170 and 30 K we see activated behavior with the transport gap $E_g \simeq 5$ meV; a fit to the activated behavior is shown in Fig. 1. At the lowest temperatures the gap appears to decrease down to $\simeq 0.43$ meV, pointing to a contribution from activation of donor (acceptor) levels, and the metallic surface states. In comparison with previously reported results,[14,15] our
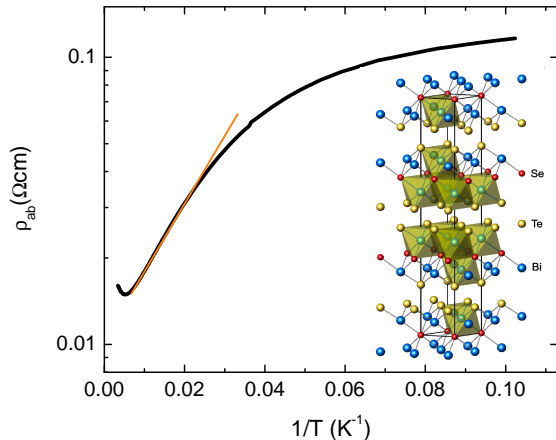
FIG. 1. (Color online) Arrhenius plot of the in-plane resistivity of Bi_2Te_2Se, log ρ vs $1/T$. The straight line is a fit to the activated hopping formula, $\rho = \rho_0 \exp[E_g/(k_B T)]$, between 30 and 170 K. Inset: The unit cell illustrating the quintuple Te–Bi–Se–Bi–Te layers stacked along the c axis.

sample has a smaller activation energy; previous reports are in the range $20 - 23$ meV. The residual resistivity at low temperatures is $10-50$ times smaller than in the previous reports.[14,15] However, the transport gaps observed in other works in the $T \rightarrow 0$ K limit are much smaller, $\simeq 4\,\mu eV$, hinting at a more significant contribution from activation of donor/acceptor levels and the surface states than in our sample. The difference in transport properties is probably related to minute stoichiometry differences. The measurement of thermopower on a sample from the same batch showed that the charge carriers in the sample are electrons.[35]

A.   Energy gap

The temperature dependence of the reflectance of Bi_2Te_2Se for the light polarized in the a-b plane is shown over a wide frequency range in Fig. 2(a); the region close to the band edge is shown in more detail in Fig. 2(b) at 295 K. The reflectance in the far infrared displays a weakly metallic character and is dominated by a strong low-frequency phonon mode. A weaker phonon mode can be distinguished above 100 cm^{-1} as a small notch superimposed on the stronger feature. At higher energies structures due to the gap edge at $E_g \simeq 300$ meV and several interband transitions are clearly visible in the reflectance. In addition, some of these features have a pronounced temperature dependence.

The real part of the optical conductivity (σ_1) has been determined from a Kramers-Kronig analysis of the reflectance and is shown over a wide range in Fig. 3. The most prominent features are the strongly temperature-
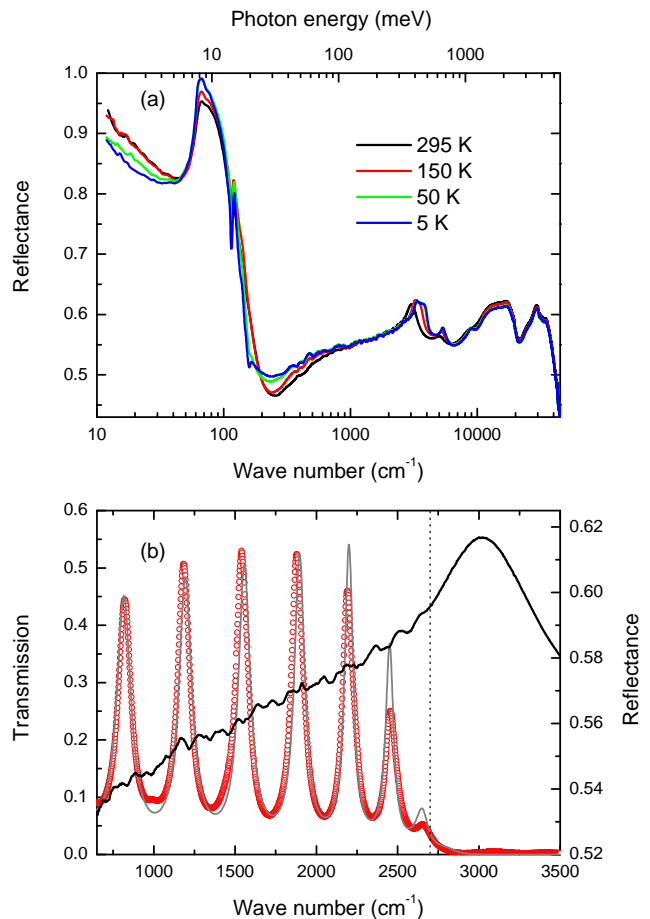

FIG. 2. (Color online) (a) Reflectivity of Bi_2Te_2Se over a wide frequency range for light polarized in the a-b planes at several temperatures. (b) Transmission through a cleaved flake $\simeq$ 2 μm thick compared to the bulk reflectance at 295 K. Open red symbols are the measured values of transmission, and the thin grey line is fit using the Tauc-Lorentz model. The dotted line indicates the point at which the sample becomes opaque.

dependent interband absorptions associated with the band edge and a very strong low-energy vibration at $\simeq 62$ cm^{-1}. From σ_1 the optical band gap can be roughly estimated to $E_g \simeq 2400$ cm^{-1} (300 meV) at 295 K. The onset of the gap in Bi_2Te_2Se is much sharper than in Bi_2Se_3,[22] where the natural Se deficiency results in intrinsic doping and a well-defined metallic (Drude-like) contribution. It may be noted that the transport gap extracted from the resistivity measurement is almost two orders of magnitude smaller than the optical band gap, which suggests that conduction occurs as a result of hopping through localized impurity states within the gap.

An improved estimate of the band gap may be obtained from combining the reflectance and transmission measurements. A comparison of the reflectance of the bulk material and the transmission through a thin sample at 295 K is shown in Fig. 2(b). Strong Fabry-Perot oscillations are observed in the transmission in the mid-
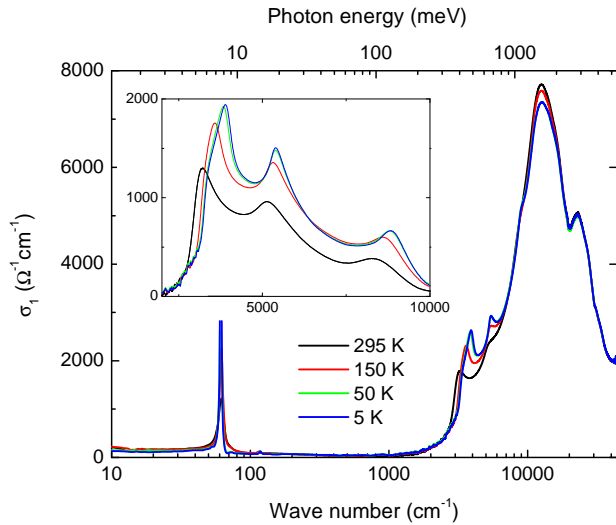
FIG. 3. (Color online) Optical conductivity in the planes of Bi_2Te_2Se over a wide energy range for several different temperatures. Inset: Optical conductivity in the mid-infrared and near-infrared regions with the contribution from the high-frequency oscillators removed.

infrared region; however, weak fringes are also observed in the reflectance. The explanation for this is that the sample cleaves extremely easily and its surface inevitably terminates in thin flakes. A part of the incident light is reflected while another part is transmitted through the flake and reflected from the back surface; the back reflection interferes with the primary reflection and produces fringes. A dashed vertical line at 2700 cm^{-1} (335 meV) indicates where the Fabry-Perot oscillations in both the reflectance and transmission appear to terminate. The transmission data has been fit using a Tauc-Lorentz model[36] for the dielectric function in which a modified Lorentzian oscillator [see Eq. (2)] is used to describe the interband absorptions; the imaginary part is written as

$$\epsilon_{2,\mathrm{TL}} = \begin{cases} \left[\dfrac{A\,\Gamma\omega_0(\omega - E_g/\hbar)^2}{(\omega^2 - \omega_0^2)^2 + \Gamma^2\omega^2} \cdot \dfrac{1}{\omega} \right], & \hbar\omega > E_g, \\ 0, & \hbar\omega \leqslant E_g. \end{cases} \quad (1)$$

The fitted parameters A, Γ, $\hbar\omega_0$ and E_g correspond to the intensity, broadening, transition energy, and energy gap, respectively. The real part is determined from a Kramers-Kronig analysis of $\epsilon_{2,\mathrm{TL}}$, allowing the transmission to be calculated for a thin slab.[37] Pieces of varying thickness ($\simeq 0.8 - 9$ μm) have been examined, and the fit to the transmission through a 2 μm thick flake of Bi_2Te_2Se is shown in Fig. 2(b). The band gap was determined in samples with several different thicknesses to be $E_g \approx 285$ meV [$E_g/(2\pi\hbar c) \approx 2300$ cm^{-1}], which is somewhat lower than the energy at which the fringes are observed to disappear.
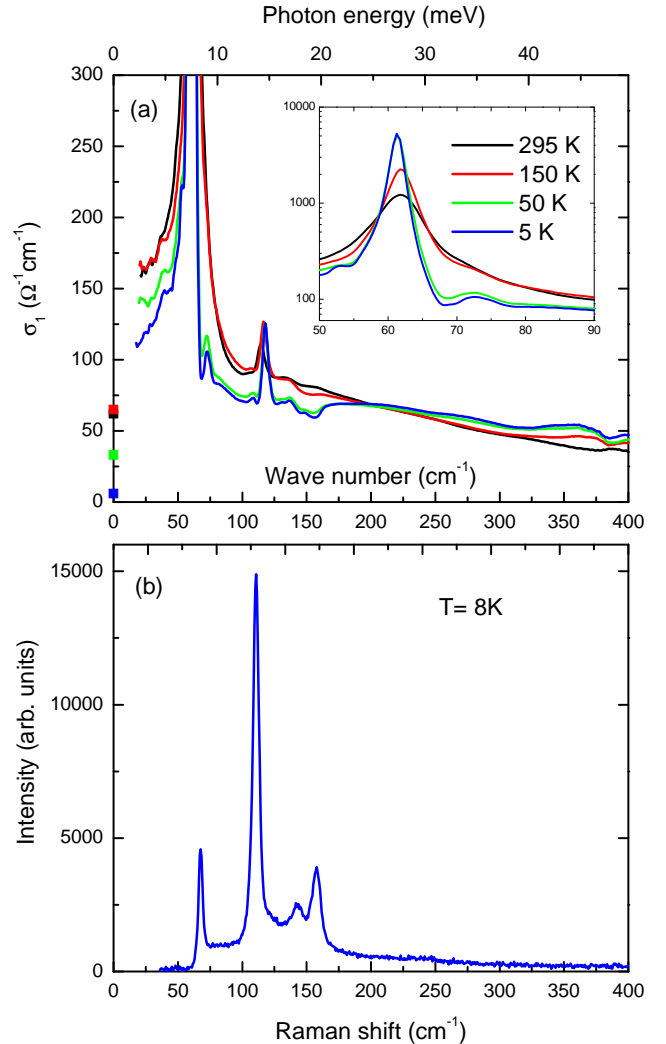
The optical properties of the bulk are described us-

FIG. 4. (Color online) (a) The temperature dependence of the real part of the optical conductivity of Bi_2Te_2Se for light polarized in the planes at low energies. The symbols at the origin denote the transport values for the dc conductivity. Inset: The conductivity in the region of the strong optical phonon showing the asymmetry in the feature at low temperature. (b) The Raman response at 8 K.

ing the Drude-Lorentz model for the complex dielectric function

$$\tilde{\epsilon}(\omega) = \epsilon_\infty - \frac{\omega_{pD}^2}{\omega^2 + i\omega/\tau_D} + \sum \frac{\Omega_j^2}{\omega_j^2 - \omega^2 - i\omega\gamma_j}, \quad (2)$$

where ϵ_∞ is the real part of the dielectric function at high frequency, $\omega_{p,D}^2 = 4\pi ne^2/m^*$ and $1/\tau_D$ are the square of the plasma frequency and scattering rate for the delocalized (Drude) carriers, respectively, and m^* is an effective mass. For the Lorentz oscillators ω_j, γ_j and Ω_j represent the position, width, and strength of the jth vibration or excitation. The complex conductivity is $\tilde{\sigma} = \sigma_1 + i\sigma_2 = -i\omega[\tilde{\epsilon}(\omega) - \epsilon_\infty]/4\pi$. In addition to the vibrational parameters, discussed in Sec. III B, a fit to the

low-frequency conductivity at room temperature yields $\omega_{pD} \simeq 1300$ cm^{-1} and $1/\tau_D \simeq 200$ cm^{-1}; this value for the plasma frequency corresponds to a carrier concentration of $n/m^* \simeq 1.7 \times 10^{18}$ cm^{-3}, consistent with previous results.[10]

One of the more interesting aspects of this material is the unusual temperature dependence of the interband transition associated with the gap edge, shown in Fig. 3, in which the increase in intensity, or spectral weight (defined as the area under the conductivity curve over a given frequency interval) of this feature, or set of features, in the $2500 - 7000$ cm^{-1} region, is compensated for by a loss of spectral weight at high frequency. This behavior may be shown in more detail by fitting the strong high-frequency features at $\simeq 13\,000$ and $24\,000$ cm^{-1} and then subtracting this contribution from the conductivity. The result of this procedure is shown in the inset of Fig. 3. At low temperature the peak of the lowest interband absorption hardens by $\simeq 700$ cm^{-1} and develops a weak shoulder, while the two higher-energy features appear symmetric and display smaller blue shifts. The gap edge appears to harden by $\simeq 430$ cm^{-1}.

The thermal shifts in the gap edge and the absorption peaks are significant. One effect of the decrease in temperature is that the lattice contracts, which leads to an increase in the band gap.[38] However, a more important process is the phonon absorption and re-emission. The highest-energy phonons in the system (Sec. III B) set a temperature scale of approximately 170 K. When the temperature is much lower than this, the phonon processes become inaccessible and the gap increases. While the strong temperature dependence of the gap may be understood with phonons, the unusual shifts of the interband absorptions are more likely linked to the contraction of the lattice.

At long wavelengths the optical conductivity is consistent with the dc transport: the conductivity is very small and it further decreases as temperature is lowered. As shown in Fig. 4(a), the values of σ_1 extrapolate roughly to the values of the dc conductivity. Since the dc conductivity at low temperatures is finite, there is also a weak free-carrier (Drude-like) contribution. However, it is impossible to accurately model this since it is masked by larger effects; a strong background which peaks around the 62 cm^{-1} phonon and persists up to at least 400 cm^{-1}. A part of this broad background may be identified as a far-infrared band due to the presence of impurities. The impurity band is slightly enhanced as the temperature is lowered. This is in agreement to what was previously reported in Bi$_2$Te$_2$Se and attributed to impurities.[23] A similar impurity band was also observed several years ago in a series of doped semiconductors, Si:P.[39] The presence of impurity states in the low-energy excitations agrees with the small transport gap obtained from the resistivity measurement. A wide impurity band is centered at $200 - 300$ cm^{-1}, but there may be another impurity band centered at $30 - 40$ cm^{-1} ($\sim 4 - 5$ meV), lying in the side band of the strong optical phonon. While the latter impurity band would agree with the small activation energy obtained in the resistivity measurement, it is possible that this feature is instead linked to the strong low-lying E_u phonon, discussed in the following Section.

B. Vibrational properties

The optical conductivity of Bi$_2$Te$_2$Se allows the vibrational properties to be analyzed. As Fig. 4(a) shows, only two sharp phonon peaks are observed at room temperature. At low temperatures these vibrations further sharpen, but in addition several other, albeit much weaker, modes appear. The symmetry group analysis of Bi$_2$Te$_2$Se in the $R\bar{3}m$ setting gives the irreducible vibrational representation[21,40]

$$\Gamma_{vib} = 2A_{1g} + 2E_g + 2A_{2u} + 2E_u. \qquad (3)$$

Here, the A_{1g} and E_g modes are Raman-active. The A_{2u} and E_u modes are infrared active along the c axis and the a-b planes, respectively. The two E_u modes can be identified as the two strong vibrations observed at 62 cm^{-1} and 117 cm^{-1}.[41] As the temperature is decreased, the low-energy mode softens, while the higher-energy mode hardens. At low temperatures the 62 cm^{-1} mode, shown in the inset of Fig. 4(a), appears to develop a slight asymmetry, with a tail at low frequencies. An inhomogeneous structure would be enough to cause an asymmetry in such a strong phonon mode; however, small level shifts in the reflectance can also artificially produce an asymmetry in the line shape of a strong phonon in an insulator.

The infrared-active modes observed at 5 K have been fit to Lorentz oscillators with a polynomial background and the frequencies, widths and strengths are listed in Table I. Contrary to previous experiments on Bi$_2$Se$_3$,[22] we can find no convincing evidence of Fano-like behavior in the strong phonon at $\simeq 62$ cm^{-1}. In addition to the two allowed in-plane infrared modes, there are at least seven other infrared-active modes observed. It is possible that disorder may lead to the lifting of the degeneracy of the E_u modes, leading to weak splitting. However, we note that the fit to the conductivity by employing two resonances at $\simeq 137$ and 149 cm^{-1} may actually be improved by considering two Fano antiresonances[42] at $\simeq 144.1$ and 155.8 cm^{-1}, respectively. The Raman spectrum is shown at 8 K in Fig. 4(b). The energies of the Raman-active modes are very close to the energies of some of the weak phonons that appear in the conductivity at low temperature; it is possible that symmetry breaking may lead to the activation of Raman modes that are normally not infrared active. In particular the positions of the two antiresonances in the conductivity are very close to the two high-frequency Raman modes at 142 and 158 cm^{-1} (Table I). In low-dimensional materials, the totally-symmetric A_{1g} Raman modes have been observed to undergo out-of-phase coupling to produce an optically-active mode at the same frequency as the Raman mode;[43] in systems where these modes sit upon

TABLE I. The fitted parameters for the infrared-active modes in the optical conductivity at 5 K and the Raman-active modes at 8 K. The estimated errors are indicated in parenthesis. With the exception of the Raman intensities, all units are cm^{-1}.

	Infrared[a]		
mode	ω_j	γ_j	Ω_j
	51.6 (0.1)	8.3 (0.7)	133 (11)
E_u	61.7 (0.03)	2.0 (0.1)	936 (25)
	72.7 (0.04)	7.0 (0.3)	114 (4)
	108.0 (0.1)	6.1 (0.7)	40 (4)
E_u	117.8 (0.02)	6.0 (0.1)	159 (2)
	137.1 (0.08)	8.5 (0.5)	55 (2)
	149.0 (0.09)	5.0 (0.5)	22 (2)
	(Antiresonance[b])		
	144.1 (0.1)	9.0 (0.5)	68 (3)
	155.8 (0.1)	13.1 (0.8)	100 (4)
	Raman		
mode	ω_j	γ_j	I/I_0
A_{1g}/E_g	67.7 (0.1)	3.5 (0.2)	0.21
A_{1g}/E_g	110.7 (0.1)	5.1 (0.1)	1.00
A_{1g}/E_g	142.2 (0.5)	19.6 (3.5)	0.35
A_{1g}/E_g	157.7 (0.2)	7.1 (0.4)	0.27

[a] Two very weak modes at ≈ 39 and 85 cm^{-1} are identified but not fit.

[b] The modes at 137.1 and 149 cm^{-1} are fit using antiresonances.

a strong electronic background they appear as antiresonances rather than resonances.[44] A similar mechanism may be responsible for the Fano-like line shapes observed in this material. Since we seem to observe at least nine modes in total, it is also possible that the A_{2u} out-of-plane modes may also be activated by disorder or a slight misalignment; these vibrations typically manifest themselves in the planes at the longitudinal-optic positions.[45] Overall, the low-energy optical and vibrational properties of Bi$_2$Te$_2$Se point towards the importance of substitutional disorder and intrinsic doping.

C. Pressure

The structure of Bi$_2$Te$_2$Se appears to be "soft" or easily compressible along the c-axis, where the quintuple atomic layers are linked by weak van der Waals interaction (inset of Fig. 1). A natural question is how sensitive this material is to pressure. Indeed, the changes in the gap under pressure in the related compounds Bi$_2$Te$_3$ and Bi$_2$Se$_3$ suggest that hydrostatic pressure is very effective at tuning the band structure. In Bi$_2$Te$_3$, Vilaplana et $al.$[46] report reducing the gap from 170 to 120 meV by applying 6 GPa. In Bi$_2$Se$_3$ the optical gap is increased from 170 meV at ambient pressure to 450 meV at 8 GPa.[47]

In Fig. 5(a), log(1/t) is plotted as a function of frequency for different pressures at room temperature. Transmission through a thin film of thickness d is given
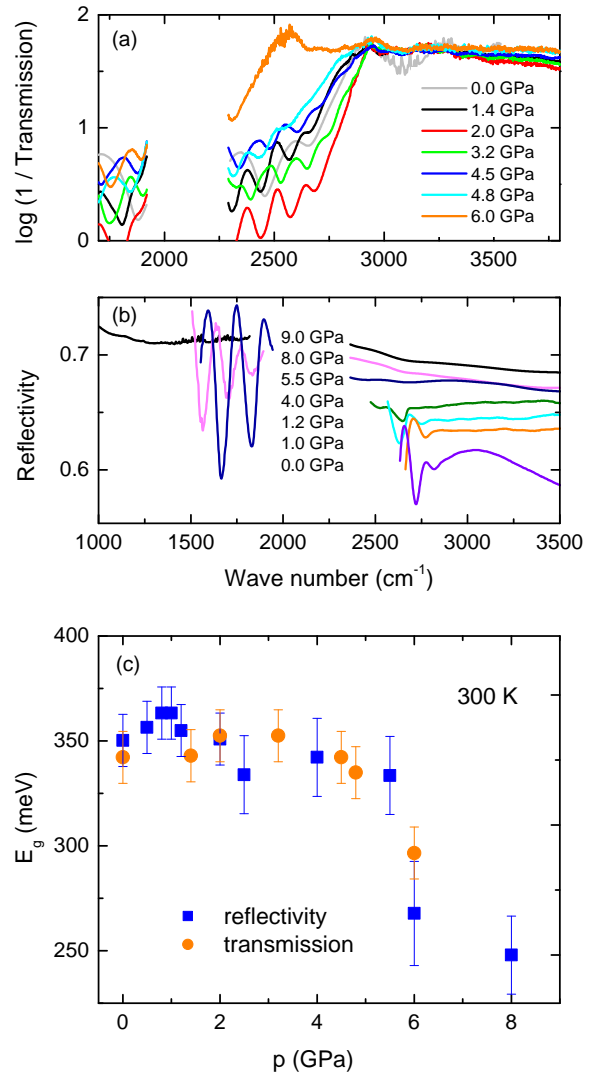

FIG. 5. (Color online) The frequency dependence at room temperature of (a) the log of the inverse transmission and (b) the reflectivity, for a thin flake of Bi$_2$Te$_2$Se at various pressures. The spectral range between 2000 – 2300 cm^{-1} is not shown due to the strong absorptions of the diamond in this region. (c) The comparison of the pressure dependence of the bulk band gap E_g determined from reflectivity and transmission measurements.

by[48]

$$t(\omega) \approx \frac{1}{1 + 4\pi d\sigma_1(\omega)/c} \qquad (4)$$

so that 1/t represents an approximation to the real part of the conductivity, offset by a constant. The gap may be simply estimated as the energy at half of the maximum value of 1/$t(\omega)$. The oscillations below the gap edge are caused by the Fabry-Perot interference, previously illustrated in Fig. 2(b). The pressure dependence of the gap may also be obtained from the reflectivity measurements,
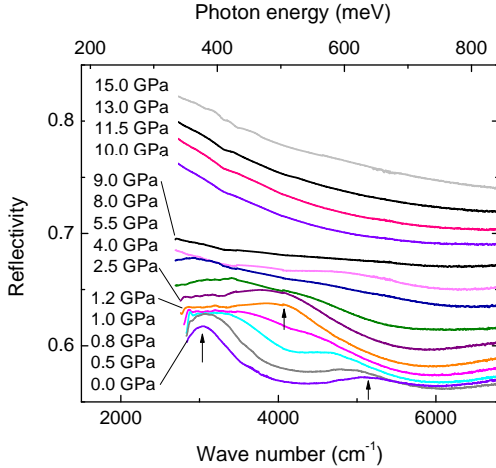
FIG. 6. (Color online) The detailed pressure dependence of the reflectivity of Bi_2Te_2Se at room temperature. The arrows indicate the location of features associated with interband absorptions.

FIG. 7. (Color online) First principles calculations (including spin-orbit coupling) of the real part of conductivity, σ_1, for various lattice compressions along the c axis. Inset: Comparison of calculated σ_1 and the measured optical conductivity at 5 K at ambient pressure.

shown in Fig. 5(b). Below the gap edge, strong Fabry-Perot oscillations appear and the energy of their onset may be taken as the value of the gap. Fig. 5(c) shows the pressure dependence of the gap determined from the transmission and reflectivity measurements as described above; the two estimates agree very well.

Up to 4 GPa, the effect of pressure on the gap edge in Bi_2Te_2Se is fairly modest, especially when compared to Bi_2Te_3 or Bi_2Se_3.[46,47] However, a steep decrease in the gap value begins above 4 GPa, and by 8 GPa the gap has moved from ~ 340 to ~ 250 meV. A wider spectral range for the reflectivity measured under pressure is shown in Fig. 6. For clarity, only the data above ~ 2800 cm^{-1} is shown. Already below 1 GPa, the reflectivity changes significantly as pressure is applied. At the lowest pressures, up to 0.8 GPa, the two lowest interband transitions at $\simeq 3000$ and 5000 cm^{-1} are still distinguishable. As the pressure increases to 1.0 GPa, these two peaks merge into a single peak at $\simeq 4000$ cm^{-1}. When the pressure is further increased, the reflectivity level increases. Above $p \simeq 9 - 10$ GPa the gap can no longer be followed. Extrapolating the data in Fig. 5 the system is expected to become metallic above 10 GPa.

In order to compare our data with the band structure predictions, the inset of Fig. 7 shows a comparison between the experimentally determined σ_1 at 5 K and the calculated σ_1 for an uncompressed lattice. Overall, the agreement is quite good and the value of the gap is approximately correct. The absorption bands are all reproduced, despite a minor shift in frequency.

The main panel of Fig. 7 shows the calculated conductivity σ_1 for different lattice compressions. The effect of pressure on this layered structure was simulated as a re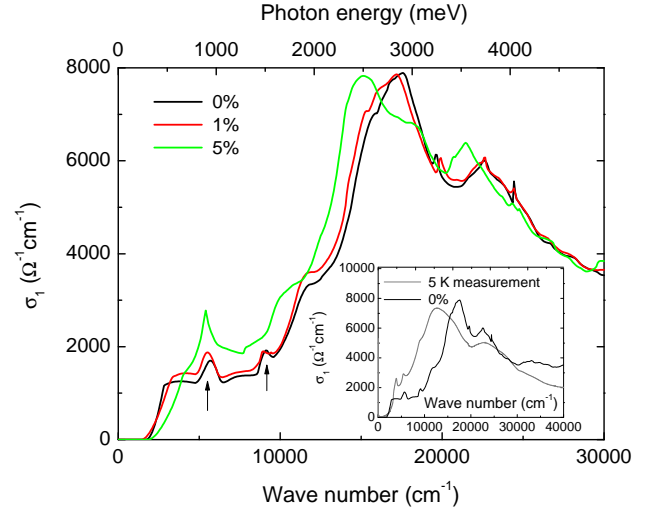duction of inter-planar distances along the c axis while keeping the a-b plane lattice parameters constant. In this way we only change the distance between quintuple layers, linked by van der Waals interactions. All the other bonds are covalent and therefore much less compressible. The calculated gap edge does not significantly depend on c-axis compression. On the contrary, the absorptions above the gap edge, marked by arrows in Fig. 7, show pressure dependence. For 5% compression of the c axis, only one peak remains below 10 000 cm^{-1}. This agrees with the reflectivity under pressure, which shows that the two structures below 6000 cm^{-1} merge into one for pressures above 1.0 GPa.

Overall, the high-pressure behavior of optical properties in Bi_2Te_2Se suggests that its band structure is very sensitive to pressure. The collapse of the gap does not seem to be captured by the LDA calculations in which only c-axis compression is considered. This indicates that the changes of the geometry within a quintuple layer may play an important role in the closing of the gap under pressure.

IV. CONCLUSIONS

The optical properties of Bi_2Te_2Se have been determined over a wide temperature and frequency range. The far-infrared optical conductivity indicates the presence of an impurity band at $\simeq 200$ cm^{-1} (25 meV), well below the band gap. Numerous in-plane vibrational modes can be identified at 5 K in Bi_2Te_2Se, at least seven more than what is allowed by symmetry. Both the extra phonon modes and the impurity band are consistent with presence (and importance) of disorder and symmetry break-

ing in this material.

The band gap edge is determined to be $E_g \simeq 300$ meV at room temperature. At low temperatures E_g shifts strongly to higher energies. Similarly, several interband transitions or absorptions above the gap edge show strong temperature dependence. Their behavior indicates that the band structure is significantly influenced by thermal contraction of the lattice.

The high-pressure optical properties of Bi_2Te_2Se have been determined at room temperature. A strong suppression of the gap edge occurs above 4.5 GPa. Commencing at low pressures, $p < 1.0$ GPa, absorptions above the gap edge show a strong pressure dependence. Our measurements are in reasonable agreement with LSDA calculations.

ACKNOWLEDGMENTS

* ana.akrap@unige.ch

† homes@bnl.gov

[1] D. Hsieh, D. Qian, L. Wray, Y. Xia, Y. S. Hor, R. J. Cava, and M. Z. Hasan, Nature (London) **452**, 970 (2008).

[2] M. Z. Hasan and C. L. Kane, Rev. Mod. Phys. **82**, 3045 (2010).

[3] J. E. Moore, Nature **464**, 194 (2010).

[4] H. Zhang, C.-X. Liu, X.-L. Qi, X. Dai, Z. Fang, and S.-C. Zhang, Nature Phys. **5**, 438 (2009).

[5] L.-L. Wang and D. D. Johnson, Phys. Rev. B **83**, 241309 (2011).

[6] M. Hasan, H. Lin, and A. Bansil, Physics **2**, 108 (2009).

[7] T. Valla, Z.-H. Pan, D. Gardner, Y. S. Lee, and S. Chu, Phys. Rev. Lett. **108**, 117601 (2012).

[8] E. Gaudin, S. Jobic, M. Evain, and R. Brec, Materials Research Bulletin **30**, 549 (1995).

[9] N. Abrikosov and V. Bankina, Zhurnal Neorganicheskoi Khimii **3**, 659 (1958).

[10] C. B. Satterthwaite and R. W. Ure, Phys. Rev. **108**, 1164 (1957).

[11] V. Kul'bachinskii, A. Kaminskii, K. Kindo, Y. Narumi, K. Suga, P. Lostak, and P. Svanda, JETP Letters **73**, 352 (2001).

[12] A. Sklenár, C. Drasar, A. Krejcová, and P. Losták, Crystal Research and Technology **35**, 1069 (2000).

[13] T. Plecháček, J. Navrátil, and J. Horák, Journal of Solid State Chemistry **165**, 35 (2002).

[14] Z. Ren, A. A. Taskin, S. Sasaki, K. Segawa, and Y. Ando, Phys. Rev. B **82**, 241306(R) (2010).

[15] S. Jia, H. Ji, E. Climent-Pascual, M. K. Fuccillo, M. E. Charles, J. Xiong, N. P. Ong, and R. J. Cava, Phys. Rev. B **84**, 235206 (2011).

[16] Z. Ren, A. A. Taskin, S. Sasaki, K. Segawa, and Y. Ando, Phys. Rev. B **85**, 155301 (2012).

[17] J. Xiong, A. Petersen, D. Qu, Y. Hor, R. Cava, and N. Ong, Physica E **44**, 917 (2012).

[18] H. Ji, J. M. Allred, M. K. Fuccillo, M. E. Charles, M. Neupane, L. A. Wray, M. Z. Hasan, and R. J. Cava, Phys. Rev. B **85**, 201103(R) (2012).

[19] M. Neupane, S.-Y. Xu, L. A. Wray, A. Petersen, R. Shankar, N. Alidoust, C. Liu, A. Fedorov, H. Ji, J. M. Allred, Y. S. Hor, T.-R. Chang, H.-T. Jeng, H. Lin, A. Bansil, R. J. Cava, and M. Z. Hasan, Phys. Rev. B **85**, 235406 (2012).

[20] T. Arakane, T. Sato, S. Souma, K. Kosaka, K. Nakayama, M. Komatsu, T. Takahashi, Z. Ren, K. Segawa, and Y. Ando, Nature Commun. **3**, 636 (2012).

[21] H. Köhler and C. R. Becker, phys. stat. sol. (b) **61**, 533 (1974); K. Unkelbach, C. Becker, H. Köhler, and A. Middendorff, Physica Status Solidi (b) **60**, K41 (1973).

[22] A. D. LaForge, A. Frenzel, B. C. Pursley, T. Lin, X. Liu, J. Shi, and D. N. Basov, Phys. Rev. B **81**, 125120 (2010).

[23] P. Di Pietro, F. M. Vitucci, D. Nicoletti, L. Baldassarre, P. Calvani, R. Cava, Y. S. Hor, U. Schade, and S. Lupi, Phys. Rev. B **86**, 045439 (2012).

[24] S. Nakajima, Journal of Physics and Chemistry of Solids **24**, 479 (1963).

[25] P. Bayliss, Amer. Mineral. **76**, 257 (1991).

[26] C. C. Homes, M. Reedyk, D. A. Crandles, and T. Timusk,

[27] Appl. Opt. **32**, 2976 (1993).

[27] M. Dressel and G. Grüner, *Electrodynamics of Solids* (Cambridge University Press, Cambridge, 2001).

[28] F. Wooten, *Optical Properties of Solids* (Academic Press, New York, 1972) pp. 244–250.

[29] F. Datchi, A. Dewaele, P. Loubeyre, R. Letoullec, Y. Le Godec, and B. Canny, High Pressure Research **27**, 447 (2007).

[30] P. Lerch, L. Quaroni, J. Wambach, J. Schneider, D. Armstrong, D. Rossetti, F. Mueller, P. Peier, V. Schlott, L. Carroll, P. Friedli, H. Sigg, S. Stutz, and M. Tran, Journal of Physics: Conference Series **359**, 012003 (2012).

[31] S. Y. Savrasov, Phys. Rev. B **54**, 16470 (1996).

[32] J. P. Perdew, K. Burke, and M. Ernzerhof, Phys. Rev. Lett. **77**, 3865 (1996).

[33] P. Larson, V. A. Greanya, W. C. Tonjes, R. Liu, S. D. Mahanti, and C. G. Olson, Phys. Rev. B **65**, 085108 (2002).

[34] X.-Q. Dai, B. Zhao, J.-H. Zhao, Y.-H. Li, Y.-N. Tang, and N. Li, Journal of Physics: Condensed Matter **24**, 035502 (2012).

[35] A. Akrap, A. Ubaldini, E. Giannini, and L. Forró, arXiv:1210.3901v1 (2012).

[36] G. E. Jellison and F. A. Modine, Appl. Phys. Lett. **69**, 371 (1996); Appl. Phys. Lett. **69**, 2137 (1996).

[37] A. Kuzmenko, computer code, RefFIT (University of Geneva, Geneva, Switzerland).

[38] P. Lautenschlager, P. B. Allen, and M. Cardona, Phys. Rev. B **31**, 2163 (1985).

[39] A. Gaymann, H. P. Geserich, and H. v. Löhneysen, Phys. Rev. B **52**, 16486 (1995).

[40] W. Richter and C. R. Becker, phys. stat. sol. (b) **84**, 619 (1977).

[41] W. Cheng and S.-F. Ren, Phys. Rev. B **83**, 094301 (2011).

[42] C. C. Homes, T. Timusk, D. A. Bonn, R. Liang, and W. N. Hardy, Can. J. Phys. **73**, 663 (1995).

[43] M. J. Rice, Phys. Rev. Lett. **37**, 36 (1976).

[44] C. S. Jacobsen, D. B. Tanner, and K. Bechgaard, Phys. Rev. B **28**, 7019 (1983).

[45] M. Reedyk and T. Timusk, Phys. Rev. Lett. **69**, 2705 (1992).

[46] R. Vilaplana, O. Gomis, F. J. Manjón, A. Segura, E. Pérez-González, P. Rodríguez-Hernández, A. Muñoz, J. González, V. Marín-Borrás, V. Muñoz Sanjosé, C. Drasar, and V. Kucek, Phys. Rev. B **84**, 104112 (2011); R. Vilaplana, D. Santamaría-Pérez, O. Gomis, F. J. Manjón, J. González, A. Segura, A. Muñoz, P. Rodríguez-Hernández, E. Pérez-González, V. Marín-Borrás, V. Muñoz Sanjose, C. Drasar, and V. Kucek, Phys. Rev. B **84**, 184110 (2011).

[47] Segura, A. and Panchal, V. and Sánchez-Royo, J. F. and Marín-Borrás, V. and Muñoz-Sanjosé, V. and Rodríguez-Hernández, P. and Muñoz, A. and Pérez-González, E. and Manjón, F. J. and González, J., Phys. Rev. B **85**, 195139 (2012).

[48] E. van Heumen and D. van der Marel, in *Lectures on the Physics of Strongly Correlated Systems XI: Eleventh Training Course in the Physics of Strongly Correlated Systems*, edited by F. Mancini and A. Avella (AIP Conference Proceedings 918, 2006).